

Intrinsic anomalous Hall effect in ferromagnetic metals studied by the multi-*d*-orbital tight-binding model

Hiroshi KONTANI¹, Takuro TANAKA¹ and Kosaku YAMADA²

¹*Department of Physics, Nagoya University, Furo-cho, Nagoya 464-8602, Japan.*

²*Engineering, Ritsumeikan University, 1-1-1 Noji Higashi, Kusatsu, Shiga 525-8577, Japan.*

(Dated: October 10, 2018)

To elucidate the origin of anomalous Hall effect (AHE) in ferromagnetic transition metals, we study the intrinsic AHE based on a multi-orbital ((d_{xz}, d_{yz})) tight-binding model. We find that a large anomalous velocity comes from the off-diagonal (inter-orbital) hopping. By this reason, the present model shows a large intrinsic anomalous Hall conductivity (AHC) which is compatible with typical experimental values in ferromagnets [$10^2 \sim 10^3 \Omega^{-1} \text{cm}^{-1}$], without necessity to assume a special band structure at the Fermi level. In good metals where ρ is small, the intrinsic AHC is constant (dissipation-less) as found by Karplus and Luttinger. In bad metals, however, we find that the AHC is proportional to ρ^{-2} when $\hbar/2\tau$ is larger than the minimum band-splitting measured from the Fermi level, Δ . This crossover behavior of the intrinsic AHE, which was first derived in J. Phys. Soc. Jpn. **63** (1994) 2627, is recently observed in various ferromagnetic metals universally by A. Asamitsu et al. We also stress that the present (d_{xz}, d_{yz})-tight binding model shows a huge spin Hall effect in a paramagnetic state.

PACS numbers: 72.10.-d, 72.80.Ga, 72.25.Ba

I. INTRODUCTION

A. Motivation and Purpose of the Study

For a long time, the anomalous Hall effect (AHE) attracts increasing attraction from both theoretical and experimental viewpoint. In general, the Hall resistivity is given by $\rho_H = R_H^0 B + 4\pi R_H^a M$, where B is the magnetic field and R_H^0 is the ordinary Hall coefficient due to the Lorentz force. R_H^a is the anomalous Hall coefficient in the presence of magnetization M . In ferromagnets, R_H^a is usually at least one order of magnitude larger than R_H^0 . In paramagnetic heavy fermion (HF) systems, ρ_H/B takes a huge value due to the AHE since the uniform susceptibility $M/B = \chi$ in HF is about $10^2 \sim 10^3$ times larger than that in usual metals owing to the strong Coulomb interaction.

Recently, the AHE in transition metal ferromagnets has been intensively studied experimentally. For example, the AHE in ferromagnetic Pyrochlore oxides shows interesting behaviors [1–4]. The AHE is also observed in ferromagnetic spinels [5] and in Ru, Ti oxides [6, 7]. Several multilayer systems [8, 9] also show distinct AHE. The AHE in spin glass systems had been discussed in refs. [10, 11].

The theoretical study of AHE was initiated by Karplus and Luttinger (KL) [12] in 1954. They found that the anomalous Hall conductivity (AHC) σ_{xy}^a ($= R_H^a M / \rho^2$) is finite and dissipation-less (i.e., σ_{xy}^a is independent of resistivity ρ) when $M \neq 0$. This KL-term is called the “intrinsic AHE” because it exists independent of impurities. In 1958, Smit presented a mechanism of “extrinsic AHE” [13]: He found that spin polarized electrons are scattered asymmetrically around an impurity in the presence of spin-orbit coupling. The AHC due to this skew-scattering mechanism is linearly proportional to ρ if

elastic scattering is dominant. The above two works were reproduced and refined in a unified way by Luttinger [14] by using the transport theory of Kohn and Luttinger, and his work were also reproduced by linear-response theory using diagrammatic technique [15, 16]. In 1970, Berger proposed another mechanism of extrinsic AHE, the side jump due to impurities [17]. This mechanism gives the AHC in proportion to ρ^2 . Note that the extrinsic AHE vanishes in a clean system without impurity.

For a long time, the AHE had been generally regarded as an extrinsic effect, and the intrinsic AHE proposed by KL had been underestimated. This would be because the theoretical model assumed in ref. [14] was too oversimplified. Moreover, ref. [14] could not offer a specific expression for σ_{xy}^a . Recently, however, various experiments suggest that the intrinsic AHE $\sigma_{xy}^a \propto (\rho)^0$ is dominant in many transition metal ferromagnets [5, 18] even in good metals with $\rho \sim 1 \mu\Omega\text{cm}$: It is surprising because the extrinsic AHC ($\propto \rho^{-1}$) should be dominant when ρ is small, if inelastic scattering is negligibly small. We here remind readers that the extrinsic AHC is very sensitive to the statistical property of impurity potential V ; For instance, it vanishes when the average value of V^3 is zero [19].

After Luttinger’s work [14], theory of intrinsic AHE has been developed by many authors. In general, σ_{xy} is composed of the “Fermi surface term” and the “Fermi sea term”; the latter comes from quasiparticles inside of the Fermi sea, and it could exist even in insulators [20]. (Note that the conductivity σ_{xx} is composed of only the Fermi surface term.) The term of the AHC derived by KL is a part of the “Fermi sea term”. Recently, M. Onoda and Nagaosa [24] and Sundaram and Niu [25] found that KL’s AHC is expressed in terms of the “Berry curvature” [24, 25]. (Note that Luttinger showed in his model that there is a term which almost cancels the Berry curvature term

[14].) On the other hand, Kontani and Yamada derived the intrinsic AHE due to the “Fermi surface term” based on the linear-response theory for the first time [26, 27]. They studied AHC in an orbitally degenerate periodic Anderson model, and succeeded in explaining the AHE in HF systems; $\sigma_{xy}^a \propto \chi$ below the coherent temperature T_0 , whereas $\sigma_{xy}^a \propto \chi \rho^{-2}$ above T_0 [28, 29]. This results explain the experimental fact that the Hall coefficients in HF systems are proportional to ρ^2 below T_0 . Miyazawa et al. proved that the intrinsic AHE also occurs in d - p models with orbital degree of freedoms [30]. Later, AHC’s for Fe and SrRuO₃ were calculated based on the LDA band calculations [31, 32].

We still have to deepen the understanding of the mechanism of AHE to explain experimental results in transition ferromagnetic metals. For example, a recent experiment by Asamitsu et al. has revealed that the intrinsic AHC ($\sigma_{xy}^a \sim 10^3 \Omega^{-1} \text{cm}^{-1}$) is observed in many ferromagnets for $\rho = 1 \sim 100 \mu\Omega\text{cm}$, whereas σ_{xy}^a starts to decrease in proportion to ρ^{-n} and $n \sim 2$ in bad metals where $\rho \gg 100 \mu\Omega\text{cm}$. This drastic crossover is reminiscent of the AHE in heavy fermion systems discussed in ref. [26]. Therefore, a detailed study based on an appropriate model for transition metals is highly required.

In the present paper, we study the intrinsic AHC in a tight-binding model with (d_{xz}, d_{yz}) -orbitals (e'_g -orbitals), which originate from the t_{2g} -orbitals (d_{xz}, d_{yz}, d_{xy}) in the tetragonal crystalline field. The band structure of this model corresponds to α and β bands of Sr₂RuO₄ [30, 33–35]. We derive a general expression for the AHC valid for any damping rate $\hbar/2\tau$, which enables us to study the AHC in bad metals. We show that the AHC is mainly given by the Fermi surface term for a wide range of $\hbar/2\tau$ since the KL’s term is canceled by another Fermi sea term in a metallic state. We also find that the anomalous velocity due to $d(xz)$ - $d(yz)$ hopping gives rise to a large AHC comparable to experimental values (about e^2/ha ; a being the lattice constant), which will be a main origin of a huge AHC in transition metal ferromagnets. In good metals, the intrinsic AHC is independent of τ as is well known. However, it becomes proportional to ρ^{-2} in bad metals where $\hbar/2\tau$ is larger than the band-splitting around the Fermi level, Δ . This crossover behavior of the AHC can explain a recent observation of the AHE by A. Asamitsu et al.

B. Origin of Intrinsic and Extrinsic AHE

Here, we shortly explain the mechanisms of both the intrinsic AHE and the extrinsic AHE in more detail: The intrinsic AHE (both Fermi surface and Fermi sea terms) originates from the interband transition of quasiparticles due to off-diagonal terms of the velocity \hat{v}_μ and the orbital angular momentum \hat{l} . (The diagrammatic expression for σ_{xy}^a is given in fig. 4.) The off-diagonal velocity contains the “anomalous velocity” (e.g. $v_x^a \propto k_y$), which gives rise to the AHE. Since it is a purely quantum effect,

it is difficult to find a simple classical analogue except for Rashba-type 2D electron gas model [36]. This might be a reason why the intrinsic AHE had been discounted for a long time. In the present model, a large anomalous velocity naturally comes from the inter-orbital (d_{xz} - d_{yz}) hopping. By this reason, atomic d -orbitals are necessary to reproduce a huge AHC in real ferromagnets.

On the other hand, the extrinsic AHE (the skew-scattering mechanism and the side-jump mechanism) happens even in a single-band model, although it is enhanced due to a multiband effect [13, 17]. Extrinsic AHCs due to skew-scattering mechanism and the side-jump mechanism are proportional to ρ^{-1} and $(\rho)^0$, respectively. The former is caused by spin-dependent asymmetric scattering around the impurity in the presence of spin-orbit coupling, and the latter is caused by lateral displacement of the wave-packet during the scattering [13, 17, 19, 37]. Diagrammatically, both skew-scattering and side-jump are expressed by *current vertex corrections* due to impurity potential, as shown in Ref. [19]. In general, detailed knowledge on the impurity potential is needed for a quantitative study of the extrinsic AHE. In the present paper, we do not study the extrinsic AHE since recent several experiments suggest that the skew scattering term is small even in good metals [5, 18].

For a long time, it was believed that the AHE is independent of the *self-energy correction* due to impurity potential. However, we show that the intrinsic AHC is reduced by the self-energy correction in bad metal. By this reason, change of the scaling law in the AHC at $\rho \sim 100 \mu\Omega\text{cm}$ reported by Asamitsu et al. [18]. is well explained in terms of the intrinsic AHE.

II. MODEL AND HAMILTONIAN

In the present paper, we study a square lattice tight-binding model with d_{xz} and d_{yz} orbitals, which is a simplified version of the (d_{xz}, d_{yz}) - p_z model. Miyazawa et al. [30] showed that the AHE exists in the latter model. However, they could not derive an explicit expression for AHC. Here, we derive explicit expressions for both the “Fermi surface term” and the “Fermi sea term” based on the present simplified model.

The ls -coupling term is indispensable for the AHE in ferromagnets: In a ferromagnetic metal with $\mathbf{M} \parallel \hat{z}$, the ls -coupling term $\lambda \mathbf{l} \cdot \mathbf{s}$ is approximately proportional to $-\lambda M \hat{l}_z$, where λ is the coupling constant. The AHE is caused by the inter-orbital transition of quasiparticles due to the off-diagonal elements of \hat{l}_z [12]. In a paramagnetic metal under B_z , on the other hand, Zeeman term for the angular momentum, $\mu_B B_z \hat{l}_z$, gives rise to the AHE [26]. Therefore, the AHE in paramagnetic metals and that in ferromagnetic ones are caused by the same transport mechanism, although the origins of magnetizations are different.

We consider that the present model with d_{xz} - and d_{yz} -orbitals describes a major part of the AHE in transi-

tion metal ferromagnets: In cubic or tetragonal crystals, $\langle \alpha | \hat{l}_z | \beta \rangle$ is nonzero only when $(\alpha, \beta) = (xz, yz)$ [$l_z = \pm 1$] and $(\alpha, \beta) = (xy, x^2 - y^2)$ [$l_z = \pm 2$]. Because levels of d_{xz} and d_{yz} orbitals are degenerate, the band structures composed of these orbitals are energetically close. This fact will be favorable to the interband hopping of quasiparticles between d_{xz} and d_{yz} orbitals, which is indispensable for the AHE. On the other hand, energy splitting between $d_{x^2-y^2}$ -orbital and d_{xy} -orbital is of the order of 1eV in square or tetragonal crystals. Therefore, the interband hopping of quasiparticles between $d_{x^2-y^2}$ - and d_{xy} -orbitals would be difficult. As a result, the main contribution to the AHE in transition metal oxides will come from the inter-orbital transition between d_{xz} - and d_{yz} -orbitals. This is the reason why we study the (d_{xz}, d_{yz}) -orbital tight-binding model.

Here, we represent the creation operator of an electron on xz (yz) orbital as $c_{\mathbf{k}}^{x\dagger}$ ($c_{\mathbf{k}}^{y\dagger}$). The Hamiltonian without ls -coupling is given by $H^0 = \sum_{\mathbf{k}} \hat{c}_{\mathbf{k}}^{\dagger} \hat{h}_{\mathbf{k}}^0 \hat{c}_{\mathbf{k}}$, where

$$\hat{h}_{\mathbf{k}}^0 = \begin{pmatrix} \xi_{\mathbf{k}}^x & \xi_{\mathbf{k}}^{xy} \\ \xi_{\mathbf{k}}^{xy} & \xi_{\mathbf{k}}^y \end{pmatrix}, \quad (1)$$

and $\hat{c}_{\mathbf{k}}^{\dagger} = (c_{\mathbf{k}}^{x\dagger}, c_{\mathbf{k}}^{y\dagger})$. $\xi_{\mathbf{k}}^x = -2t \cos k_x$, $\xi_{\mathbf{k}}^y = -2t \cos k_y$ and $\xi_{\mathbf{k}}^{xy} = 4t' \sin k_x \sin k_y$. Here, $-t$ and $\pm t'$ are the hopping integrals between nearest-neighbors and next-nearest-neighbors, respectively [34]. They are shown in fig. 1.

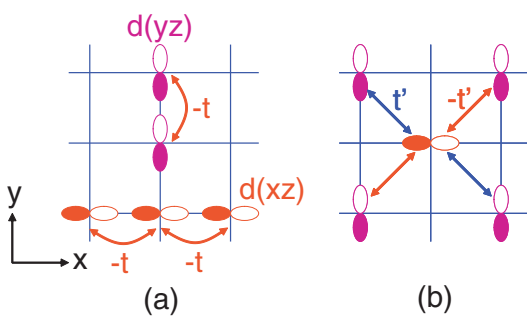


FIG. 1: (color online) (a) Hopping integrals between the same orbitals. (b) Hopping integrals between the different orbitals, which is given by the next nearest neighbor hopping. The sign of the hopping integral changes by $\pi/2$ rotation. This fact gives rise to the anomalous velocity.

Then, the velocity matrix is given by $\hat{v}_{\mu} = \partial \hat{h}_{\mathbf{k}}^0 / \partial k_{\mu}$, where $\mu = x, y$. They are given by

$$\hat{v}_x = \begin{pmatrix} 2t \sin k_x & 4t' \cos k_x \sin k_y \\ 4t' \cos k_x \sin k_y & 0 \end{pmatrix}, \quad (2)$$

$$\hat{v}_y = \begin{pmatrix} 0 & 4t' \sin k_x \cos k_y \\ 4t' \sin k_x \cos k_y & 2t \sin k_y \end{pmatrix}. \quad (3)$$

We should stress that the off-diagonal elements of \hat{v}_x , $v_x^{xy} = v_x^{yx}$, is an odd-function of k_y . In the same way, $v_y^{xy} = v_y^{yx}$ is an odd-function of k_x . They are called “anomalous velocity”. In later sections, we will show

that σ_{xy}^a is proportional to $\langle v_x^{xy} v_y^{yy} \rangle$, which can remain finite after the \mathbf{k} -summation due to the anomalous velocity. Therefore, a sizable AHC is caused by v_x^{xy} and v_y^{xy} . Atomic d -orbitals give rise to the huge AHC in transition metal ferromagnets.

To realize the AHE in ferromagnets, the atomic ls -coupling is also necessary. It is given by $H^{\lambda} = \sum_{\mathbf{k}} \hat{c}_{\mathbf{k}}^{\dagger} \hat{h}^{\lambda} \hat{c}_{\mathbf{k}}$. Because $|xz\rangle = -(|l_z = +1\rangle - |l_z = -1\rangle)/\sqrt{2}$ and $|yz\rangle = i(|l_z = +1\rangle + |l_z = -1\rangle)/\sqrt{2}i$, \hat{h}^{λ} in the present basis is given by

$$\hat{h}^{\lambda} = \text{sgn}(s_z) \lambda \hat{\tau}_y, \quad (4)$$

where λ is the coupling constant and $\hat{\tau}_y$ is the Pauli matrix for the orbital space. Note that $\hat{l}_y = \hat{l}_z = 0$ in the present basis. In Fe, $\lambda = 70\text{meV}$ [31]. Hereafter, we put $\mu_B = 1$ for the simplicity of calculation.

$$G^{\alpha\beta} = \begin{array}{c} \alpha \\ \text{---} \\ \beta \end{array}, \quad v_x^{\alpha\beta} = \begin{array}{c} \alpha \\ x \\ \text{---} \\ \beta \end{array}$$

FIG. 2: Diagrammatic expression for the Green function $G_{\alpha\beta}$ and the velocity $v_x^{\alpha\beta}$.

The Green function in the presence of atomic ls -coupling is given by $\hat{G}_{\mathbf{k}}(\omega) = (\omega + \mu - \hat{h}_{\mathbf{k}}^0 - \hat{h}^{\lambda})^{-1}$, which is given by

$$\begin{pmatrix} G_{xx} & G_{xy} \\ G_{yx} & G_{yy} \end{pmatrix} = \frac{1}{d(\omega)} \begin{pmatrix} \omega + \mu - \xi_{\mathbf{k}}^y & \alpha_{\mathbf{k}} \\ \alpha_{\mathbf{k}}^* & \omega + \mu - \xi_{\mathbf{k}}^x \end{pmatrix}, \quad (5)$$

where $\alpha_{\mathbf{k}} = \xi_{\mathbf{k}}^{xy} + i\lambda \text{sgn}(s_z)$ and $d(\omega) = (\omega + \mu - \xi_{\mathbf{k}}^x)(\omega + \mu - \xi_{\mathbf{k}}^y) - |\alpha_{\mathbf{k}}|^2$, which is expressed as

$$d(\omega) = (\omega + \mu - E_{\mathbf{k}}^+)(\omega + \mu - E_{\mathbf{k}}^-), \quad (6)$$

$$E_{\mathbf{k}}^{\pm} = \frac{1}{2} \left(\xi_{\mathbf{k}}^x + \xi_{\mathbf{k}}^y \pm \sqrt{(\xi_{\mathbf{k}}^x - \xi_{\mathbf{k}}^y)^2 + 4|\alpha_{\mathbf{k}}|^2} \right), \quad (7)$$

where $E_{\mathbf{k}}^{\pm}$ represents the quasiparticle dispersion. Figure 3 shows the Fermi surfaces for $(t, t') = (1, 0.1)$. In Sr_2RuO_4 , $t'/t \sim 0.1$ [33–35]. The electron density per spin, n , is set as 0.6 and 1.4. (Note that $t, t' < 0$ in the present Hubbard model according to Slater-Koster [40]. However, we assume $t, t' > 0$ because they are positive in Sr_2RuO_4 due to the presence of p_z -orbital between the nearest Ru-sites [33–35].) The splitting Δ^{\pm} represents the minimum band-splitting ($|E_{\mathbf{k}}^+ - E_{\mathbf{k}}^-|$) measured from the the Fermi surface of $E_{\mathbf{k}}^{\pm}$ -band. In Fig. 3, \mathbf{k}^* represents the position of the minimum band-splitting, $\Delta \equiv \min\{\Delta^+, \Delta^-\}$.

Here, we consider the quasiparticle damping rate $\gamma = \hbar/2\tau$, which is given by the imaginary part of the self-energy $\hat{\Sigma}_{\mathbf{k}}(\epsilon)$. For simplicity, we assume that γ is diagonal with respect to orbital, and independent of momentum. Then, retarded and advanced Green functions with

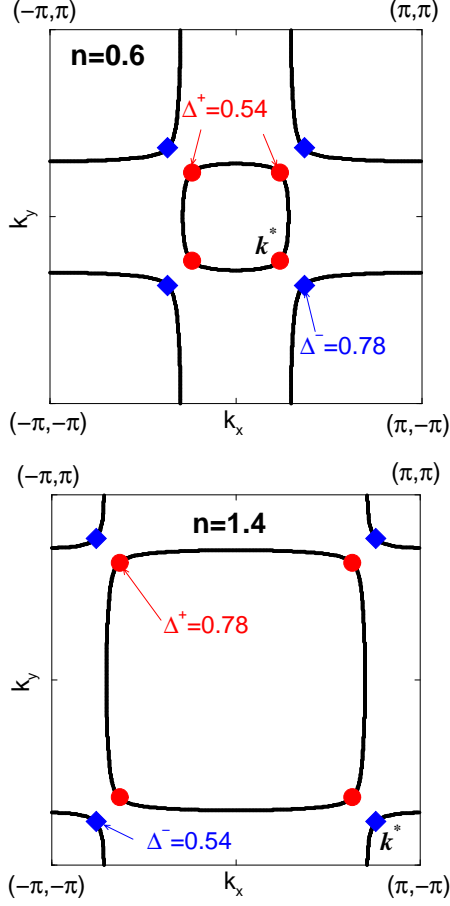


FIG. 3: (color online) Fermi surfaces for (a) $n = 0.6$ and (a) $n = 1.4$. Here we put $(t, t') = (1, 0.1)$, which corresponds to Sr_2RuO_4 .

finite γ are given by

$$G_{\alpha\beta'}^R(\omega) = G_{\alpha\beta'}(\omega + i\gamma), \quad (8)$$

$$G_{\alpha\beta'}^A(\omega) = G_{\alpha\beta'}(\omega - i\gamma), \quad (9)$$

where $\alpha, \beta = xz, yz$. This assumption will be justified when the damping is caused by local impurities since the local Green function $g_{\alpha, \beta}(\epsilon) = n_{\text{imp}} I^2 \sum_{\mathbf{k}} G_{\alpha, \beta}(\mathbf{k}, \epsilon)$ is diagonal and independent of (α, β) if $\lambda = 0$. [Offdiagonal term of $g_{\alpha, \beta}(\epsilon)$ is proportional to λ .] In the Born approximation, $\hat{\Sigma}(\epsilon) = n_{\text{imp}} I^2 \hat{g}(\epsilon)$, where n_{imp} is the impurity concentration and I is the impurity potential. The Born approximation is valid when I is much smaller than the bandwidth W_{band} . In Appendix A, we derive the AHC in the Born approximation by taking the offdiagonal term of $\hat{\Sigma}(\epsilon)$ into account correctly, and find that its effect is negligible.

On the other hand, the assumption given in eqs. (8) and (9) may not be valid in strongly correlated systems. In Appendix B and C, we study the intrinsic AHC when γ depends on momentum and band index, and find that the AHC could be changed prominently by these influences.

III. ANOMALOUS HALL CONDUCTIVITY

In this section, we derive the intrinsic AHC σ_{xy}^a (hereafter, we drop the superscript a) and the longitudinal conductivity σ_{xx} for finite quasiparticle damping rate γ based on the linear-response theory [41]. Here, we take the self-energy correction due to correlation, which causes finite quasiparticle damping rate. On the other hand, we drop all the current vertex correction (CVC). The CVC due to impurities with ls -coupling give rise to the skew scattering [19]. However, CVC due to local impurities vanishes identically. Note that the CVC due to the Coulomb interaction does not cause the skew scattering [26]. Hereafter, we put the renormalization factor $z = 1$ because z exactly cancels in the final formula of the AHC.

From now on, we assume a complete ferromagnetic state with \downarrow -spin electrons only, i.e., $\text{sgn}(s_z) = -1$. Hereafter, we drop the factor $e^2/h = 2\pi e^2/h$ (h being the Plank constant) in $\sigma_{\mu\nu}$ to simplify expressions. According to Streda [20], $\sigma_{\mu\nu}$ is given by

$$\sigma_{\mu\nu} = \sigma_{\mu\nu}^I + \sigma_{\mu\nu}^{II}, \quad (10)$$

$$\begin{aligned} \sigma_{\mu\nu}^I = & \sum_{\mathbf{k}, \alpha\alpha'\beta\beta'} \int \frac{d\epsilon}{2\pi} v_{\mu}^{\alpha'\alpha} v_{\nu}^{\beta'\beta} \left(-\frac{\partial f}{\partial \epsilon} \right) \\ & \times \left[G_{\alpha\beta'}^R G_{\beta\alpha'}^A - \frac{1}{2} (G_{\alpha\beta'}^R G_{\beta\alpha'}^R + G_{\alpha\beta'}^A G_{\beta\alpha'}^A) \right], \end{aligned} \quad (11)$$

$$\begin{aligned} \sigma_{\mu\nu}^{II} = & -\frac{1}{2} \sum_{\mathbf{k}, \alpha\alpha'\beta\beta'} \int \frac{d\epsilon}{2\pi} v_{\mu}^{\alpha'\alpha} v_{\nu}^{\beta'\beta} f(\omega) \\ & \times \left[\frac{\partial}{\partial \epsilon} G_{\alpha\beta'}^R \cdot G_{\beta\alpha'}^R - G_{\alpha\beta'}^R \frac{\partial}{\partial \epsilon} G_{\beta\alpha'}^R \right. \\ & \left. - \frac{\partial}{\partial \epsilon} G_{\alpha\beta'}^A \cdot G_{\beta\alpha'}^A + G_{\alpha\beta'}^A \frac{\partial}{\partial \epsilon} G_{\beta\alpha'}^A \right], \end{aligned} \quad (12)$$

where $v_{\mu}^{\alpha'\alpha}$ and $G_{\alpha\beta'}$ are given by eqs. (2), (3), (8) and (9). $f(\epsilon)$ is the Fermi distribution function. The diagrammatic expression is given in fig. 4 (a). We call $\sigma_{\mu\nu}^I$ and $\sigma_{\mu\nu}^{II}$ the “Fermi surface term” and the “Fermi sea term”, respectively, according to literature.

The original KL’s paper [12] studied only a part of the Fermi sea term (σ_{xy}^{IIB} given in eq. (19)), which is equivalent to the Berry curvature term. On the other hand, Kontani and Yamada [26] derived the Fermi surface term σ_{xy}^I in the $J = 5/2$ periodic Anderson model. They also showed that the Fermi sea term is absent in this model. In general models, however, both contributions exist as recognized by Luttinger [14]. Recently, a detailed analysis for both terms was given in ref. [21] for graphene. However, comparison of each term was not complete for d -electron systems. In the present paper, we show that σ_{xy}^I is much larger than σ_{xy}^{II} in metallic systems for a wide range of $\gamma = \hbar/2\tau$.

We note that the normal Hall conductivity due to the Lorentz force is proportional to γ^{-2} . In this case, σ_{xy}^I is much larger than $\sigma_{xy}^{II} \sim O(\gamma^0)$ in good metals where

$\tau = 1/2\gamma^{-1}$ is very large. On the other hand, the intrinsic AHC is of the order of γ^0 . By this reason, both σ_{xy}^I and σ_{xy}^{II} could be the same order.

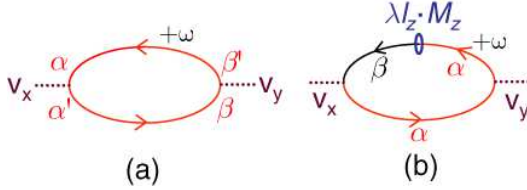


FIG. 4: (color online) (a) Diagrammatic expression for σ_{xy} . (b) First order term with respect to the atomic ls -coupling in terms of the band-diagonal representation.

From now on, we calculate the intrinsic AHC for $(\mu, \nu) = (x, y)$. First, we take the summation over $\alpha', \alpha, \beta', \beta$ in eqs. (11) and (12). After taking the \mathbf{k} -summation, only the terms $(\alpha', \alpha, \beta', \beta) = (x, x, x, y), (x, x, y, x), (x, y, x, x), (y, x, x, x)$ remain finite. Using the square lattice symmetry of the present model, we obtain that

$$\sigma_{xy}^I = \lambda \sum_{\mathbf{k}} \int \frac{d\epsilon}{2\pi} v_x^{xx} v_y^{xy} \left(-\frac{\partial f}{\partial \epsilon} \right) \frac{4\gamma}{d^R d^A}, \quad (13)$$

$$\begin{aligned} \sigma_{xy}^{II} = 2i\lambda \sum_{\mathbf{k}} \int \frac{d\epsilon}{2\pi} v_x^{xx} v_y^{xy} f(\omega) \\ \times \left[\left(\frac{1}{d^R} \right)^2 - \left(\frac{1}{d^A} \right)^2 \right], \end{aligned} \quad (14)$$

where $v_x^{xx} v_y^{xy} = 8tt' \sin^2 k_x \cos k_y$. Here, it is essential that $v_x^{xx} v_y^{xy}$ is the totally symmetric representation (A_{1g}), and it does not vanish after the \mathbf{k} -summation. Note that the term proportional to $G^R G^R + G^A G^A$ in σ_{xy}^I vanishes identically.

Here, we derive the expressions for σ_{xy}^I and σ_{xy}^{II} at $T = 0$. Then, the ω -integration in eq. (14) can be performed using the relation

$$\begin{aligned} \int_{-\infty}^{\mu} \frac{dx}{(x-a)^2(x-b)^2} = \frac{-(2\mu-a-b)}{(a-b)^2(\mu-a)(\mu-b)} \\ - \frac{2}{(a-b)^3} \ln \left(\frac{a-\mu}{b-\mu} \right) \end{aligned} \quad (15)$$

The final result for the intrinsic AHC is given by

$$\sigma_{xy} = \sigma_{xy}^I + \sigma_{xy}^{IIa} + \sigma_{xy}^{IIb}, \quad (16)$$

$$\begin{aligned} \sigma_{xy}^I = \frac{2\lambda}{\pi} \sum_{\mathbf{k}} v_x^{xx} v_y^{xy} \\ \times \frac{\gamma}{((\mu - E_{\mathbf{k}}^+)^2 + \gamma^2)((\mu - E_{\mathbf{k}}^-)^2 + \gamma^2)}, \end{aligned} \quad (17)$$

$$\begin{aligned} \sigma_{xy}^{IIa} = \frac{2\lambda}{\pi} \sum_{\mathbf{k}} v_x^{xx} v_y^{xy} \frac{1}{(E_{\mathbf{k}}^+ - E_{\mathbf{k}}^-)^2} \\ \times \text{Im} \left\{ \frac{2\mu - E_{\mathbf{k}}^+ - E_{\mathbf{k}}^- + 2i\gamma}{(\mu - E_{\mathbf{k}}^+ + i\gamma)(\mu - E_{\mathbf{k}}^- + i\gamma)} \right\}, \end{aligned} \quad (18)$$

$$\begin{aligned} \sigma_{xy}^{IIb} = \frac{4\lambda}{\pi} \sum_{\mathbf{k}} v_x^{xx} v_y^{xy} \frac{1}{(E_{\mathbf{k}}^+ - E_{\mathbf{k}}^-)^3} \\ \times \text{Im} \left\{ \ln \left(\frac{E_{\mathbf{k}}^+ - \mu - i\gamma}{E_{\mathbf{k}}^- - \mu - i\gamma} \right) \right\}. \end{aligned} \quad (19)$$

Below, we perform the numerical calculation for the AHC using eqs. (17), (18) and (19).

In the same way, we calculate the longitudinal conductivity for $\mu = \nu = x$. In this case, (12) vanishes identically, and only the Fermi surface term (11) remains finite. After taking the \mathbf{k} -summation and using the square lattice symmetry of the present model, we obtain the expression for σ_{xx} at $T = 0$ as follows:

$$\sigma_{xx} = \sigma_{xx}^{Ia} + \sigma_{xx}^{Ib}, \quad (20)$$

$$\begin{aligned} \sigma_{xx}^{Ia} = \frac{1}{2\pi} \sum_{\mathbf{k}} \{ (v_x^{xx})^2 [(\mu - \xi_y)^2 + \gamma^2] + 2(v_x^{xy})^2 \\ \times [(\xi^{xy})^2 - \lambda^2 + (\mu - \xi_y)(\mu - \xi_x) + \gamma^2] \\ + 4v_x^{xx} v_x^{xy} \xi^{xy} (\mu - \xi_y) \} / d^R(0) d^A(0), \end{aligned} \quad (21)$$

$$\begin{aligned} \sigma_{xx}^{Ib} = \frac{-1}{2\pi} \text{Re} \sum_{\mathbf{k}} \{ (v_x^{xx})^2 (\mu - \xi_y + i\gamma)^2 + 2(v_x^{xy})^2 \\ \times [(\xi^{xy})^2 - \lambda^2 + (\mu - \xi_y + i\gamma)(\mu - \xi_x + i\gamma)] \\ + 4v_x^{xx} v_x^{xy} \xi^{xy} (\mu - \xi_y + i\gamma) \} / (d^R(0))^2. \end{aligned} \quad (22)$$

Note that σ_{xx}^{II} vanishes identically. In the case of $\gamma \rightarrow 0$, σ_{xx}^{Ia} diverges as γ^{-1} whereas σ_{xx}^{Ib} is finite. Therefore, $\sigma_{xx} \sim \sigma_{xx}^{Ia}$ in good metals. However, σ_{xx}^{Ia} and σ_{xx}^{Ib} become the same order when γ is very large. We perform the numerical calculation for the σ_{xx} using eqs. (21) (22) in later sections.

Before performing the numerical study in §IV, we analyze eqs. (17), (18) and (19) when γ is very small in

detail: In this case,

$$\frac{1}{d^R(0)d^A(0)} \approx \frac{\pi}{\gamma} \frac{\delta(\mu - E_{\mathbf{k}}^+) + \delta(\mu - E_{\mathbf{k}}^-)}{(E_{\mathbf{k}}^+ - E_{\mathbf{k}}^-)^2 + \gamma^2}, \quad (23)$$

$$\begin{aligned} \text{Im} \left\{ \frac{2\mu - E_{\mathbf{k}}^+ - E_{\mathbf{k}}^- + 2i\gamma}{(\mu - E_{\mathbf{k}}^+ + i\gamma)(\mu - E_{\mathbf{k}}^- + i\gamma)} \right\} \\ \approx -\pi\delta(\mu - E_{\mathbf{k}}^+) - \pi\delta(\mu - E_{\mathbf{k}}^-), \quad (24) \\ \text{Im} \left\{ \ln \left(\frac{E_{\mathbf{k}}^+ - \mu - i\gamma}{E_{\mathbf{k}}^- - \mu - i\gamma} \right) \right\} \\ \approx -\pi\theta(\mu - E_{\mathbf{k}}^+) + \pi\theta(\mu - E_{\mathbf{k}}^-). \quad (25) \end{aligned}$$

Substituting above equations into (17)-(19), we obtain the following relation for $\gamma \rightarrow 0$:

$$\begin{aligned} \sigma_{xy}^I &\approx 2\lambda \sum_{\mathbf{k}} v_x^{xx} v_y^{xy} \\ &\times \frac{\delta(\mu - E_{\mathbf{k}}^+) + \delta(\mu - E_{\mathbf{k}}^-)}{(E_{\mathbf{k}}^+ - E_{\mathbf{k}}^-)^2}, \quad (26) \end{aligned}$$

$$\sigma_{xy}^{IIa} \approx -\sigma_{xy}^I, \quad (27)$$

$$\begin{aligned} \sigma_{xy}^{IIb} &\approx 4\lambda \sum_{\mathbf{k}} v_x^{xx} v_y^{xy} \\ &\times \frac{-\theta(\mu - E_{\mathbf{k}}^+) + \theta(\mu - E_{\mathbf{k}}^-)}{(E_{\mathbf{k}}^+ - E_{\mathbf{k}}^-)^3}. \quad (28) \end{aligned}$$

According to eq. (28), the main contribution to σ_{xy}^{IIb} comes from an area near \mathbf{k}^* in fig 3, if $E_{\mathbf{k}}^+ > 0$ and $E_{\mathbf{k}}^- < 0$ are satisfied. When $d_{\mathbf{k}} \equiv E_{\mathbf{k}}^+ - E_{\mathbf{k}}^-$ is small, then $(-\theta(\mu - E_{\mathbf{k}}^+) + \theta(\mu - E_{\mathbf{k}}^-))/d_{\mathbf{k}} \approx 2\delta(\mu - (E_{\mathbf{k}}^+ + E_{\mathbf{k}}^-)/2)$. In this case,

$$\begin{aligned} \sigma_{xy}^{IIb} &\approx 4\lambda \sum_{\mathbf{k}} v_x^{xx} v_y^{xy} \frac{\delta(\mu - (E_{\mathbf{k}}^+ + E_{\mathbf{k}}^-)/2)}{(E_{\mathbf{k}}^+ - E_{\mathbf{k}}^-)^2} \\ &\approx \sigma_{xy}^I. \quad (29) \end{aligned}$$

Note that this relation will not be satisfied in a special case where the Fermi level lies between a narrow bandgap. In the next section, we see that eq. (29) holds very well in the present model.

Here, we summarize the obtained results in this section.

(i) σ_{xy}^{IIb} was first recognized by Karplus and Luttinger [12]. It can be rewritten in terms of the summation of the Berry curvature [24].

(ii) σ_{xy}^{IIa} is another “Fermi sea term”, although its final expression (27) is written like a Fermi surface term. We find that σ_{xy}^{IIa} is very small in usual metals because σ_{xy}^{IIa} and σ_{xy}^{IIb} almost cancels each other.

(iii) The Fermi surface term is canceled by σ_{xy}^{IIa} in the clean limit, which is also recognized in 2D Dirac model [16]. However, this cancellation is imperfect when γ is finite, as shown in the next section.

Several previous works assumed that the intrinsic AHC is given by σ_{xy}^{IIb} [24, 31, 32]. One might consider that this assumption is justified by the present calculation for

$\gamma \rightarrow 0$. However, this assumption is not always guaranteed as we will see in the next section: When γ is as large as Δ , then (a) $\sigma_{xy} \approx \sigma_{xy}^I$ still holds whereas (b) σ_{xy} becomes quite different from σ_{xy}^{IIb} . In Appendix B and C, we study the intrinsic AHC in the general case where γ is \mathbf{k} -dependent or it depends on band index. In these cases, statement (a) and (b) are also true. Therefore, overall behavior of σ_{xy} for a wide range of γ is well expressed by the Fermi surface term σ_{xy}^I , not by σ_{xy}^{IIb} . This is an important result of this paper, which is obtained by considering all the terms contributing to the intrinsic AHC.

Finally, we comment that both t' and \hat{h}^λ change their signs under the gauge transformation $|xz\rangle \rightarrow -|xz\rangle$. The AHC is invariant under this gauge transformation.

IV. NUMERICAL STUDY

In this section, we perform the numerical calculation for both σ_{xy} and σ_{xx} at $T = 0$, assuming a complete ferromagnetic state where $n_\downarrow = n$ and $n_\uparrow = 0$. In this case, $m_z = \mu_B n$. (We put $\mu_B = 1$ hereafter.) The main purpose of this section is to elucidate both the filling (n) and damping rate (γ) dependences of the AHC. We perform the \mathbf{k} -summations in eq. (16) for σ_{xy} and eq. (20) for σ_{xx} numerically, dividing the Brillouin zone into 5000×5000 meshes.

The unit of conductivity in this section is e^2/ha , where h is the Plank constant and a is the unit cell length (inter-layer distance in 2D systems). If we assume the length of unit cell a is 4Å, $e^2/ha \approx 10^3 \Omega^{-1} \text{cm}^{-1}$.

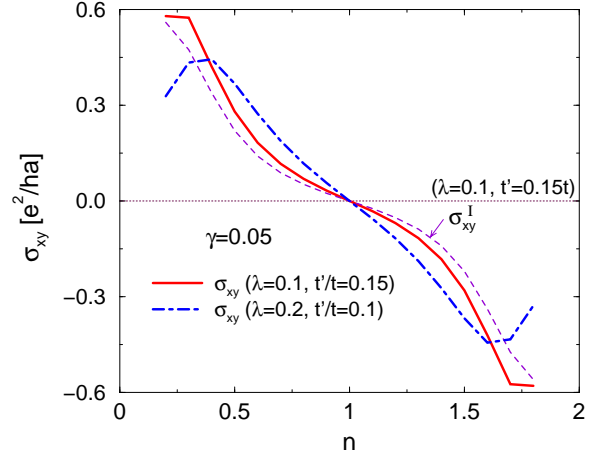


FIG. 5: (color online) Obtained total AHC (σ_{xy}) and σ_{xy}^I as a function of $n = m_z$. It is shown that $\sigma_{xy} \approx \sigma_{xy}^I$ is well satisfied. $e^2/ha \approx 10^3 \Omega^{-1} \text{cm}^{-1}$ if we put the unit cell length $a = 4\text{\AA}$. σ_{xy} is not a monotonic function of m_z , and changes its sign at $m_z \sim 1$

Figure 5 shows the n -dependence of σ_{xy} for $n = 0.2 \sim 1.8$. $n = 2$ corresponds to a ferromagnetic band insulators. In the present model, $\sigma_{xy}(n) = -\sigma_{xy}(2 - n)$. Here,

we put $\gamma = 0.05$, which is sufficiently smaller than the minimum band-splitting measured from the Fermi surface, Δ , which is shown in Fig. 3. The bandwidth of the present model is approximately $4|t| = 4$. We put the ls -coupling constant λ as $0.1 \sim 0.2$. If we assume $t = 4000\text{K}$, it corresponds to $\lambda = 400 \sim 800\text{K}$, which are realistic values in transition metals. In the present study, $|\sigma_{xy}|$ exceeds $0.5 \times 10^3 \Omega^{-1}\text{cm}^{-1}$ at $n \sim 1.8$. The obtained magnitude of $|\sigma_{xy}|$ is comparable with experimental value in Fe [31] and in SrRuO₃ [32]. Figure 6 shows the λ -dependence of $|\sigma_{xy}|$ for $n = 0.6$ and 1.4. $|\sigma_{xy}|$ is approximately proportional to λ below $\lambda \sim 0.2$, whereas it tends to saturate when λ is as large as $\Delta_{\lambda=0}$ since $\Delta = E_{\mathbf{k}^*}^+ - E_{\mathbf{k}^*}^-$ increases with λ . [31].

In Fig. 5, σ_{xy} is positive (negative) for $n < 1$ ($n > 1$); $\sigma_{xy} = 0$ at $n \approx 1$. The reason for the sign change of $\sigma_{xy} = 0$ is the following: According to eq. (16), the main contribution for σ_{xy} ($\approx \sigma_{xy}^I$ or σ_{xy}^{IIb}) comes from an area near \mathbf{k}^* . Therefore, $\sigma_{xy} \sim v_x^{xx} v_y^{xy}|_{\mathbf{k}^*} \sim tt' \sin^2 k_x^* \cos k_y^*$. Because $tt' > 0$, the sign of σ_{xy} changes to be negative when $|k_x^*| = |k_y^*|$ exceeds $\pi/2$. The sign change of the AHC as a function of m_z is actually observed in SrRuO₃.

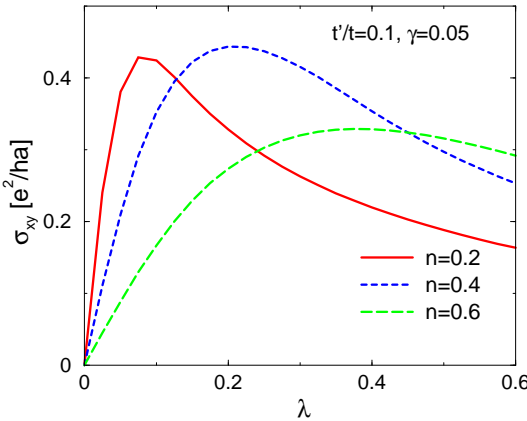


FIG. 6: (color online) λ -dependence of σ_{xy} for $n = 1.4$ and 0.6.

Next, we examine the γ -dependence of the AHC. Figure 7 shows the total AHC (σ_{xy}), σ_{xy}^I , $-\sigma_{xy}^{IIa}$ and σ_{xy}^{IIb} for $n = 1.4$. We see that all of them are γ -independent when $\gamma \ll \Delta$. On the other hand, they start to decrease with γ when $\gamma \gg \Delta$: This is easily recognized from the functional forms of eqs. (17)-(19). We see that σ_{xy}^I is almost equal to $-\sigma_{xy}^{IIa}$ and $\sigma_{xy} \approx \sigma_{xy}^{IIb}$ when $\gamma \ll \Delta$, as discussed in the previous section. On the other hand, $\sigma_{xy} \approx \sigma_{xy}^I$ whereas σ_{xy} is quite different from σ_{xy}^{IIb} for $\gamma \gg \Delta$. As a result, the Fermi surface term σ_{xy}^I succeeds in reproducing the overall behavior of the AHC for a wide range of γ . σ_{xy} is proportional to γ^{-3} for $\gamma \sim W_{\text{band}}$, which can be recognized by eq. (17).

This crossover behavior of σ_{xy} at $\gamma \sim \Delta$ was first pointed out by ref. [26]. They found that σ_{xy} is propor-

tional to γ^{-2} for $|E^f - \mu| \ll \gamma$ in $J = 5/2$ periodic Anderson model (PAM). (E^f is the energy of f -electrons.) The different γ -dependence of σ_{xy} between in d - p model and in PAM comes from the fact that the conduction bandwidth W_{band}^c is much wider than the heavy quasiparticle band in PAM. In the PAM, the quasiparticle damping is given by $\gamma = \Gamma \cdot V^2 / ((\mu - E^f)^2 + \Gamma^2)$, where V is the c - f mixing term and Γ is the imaginary part of the f -electron self-energy. Because γ saturates at $\Gamma \sim |\mu - E^f|$ and the relation $V^2 / (\mu - E^f) \sim W_{\text{band}}^c$ holds in the PAM, γ will always be smaller than W_{band}^c even if $\Gamma \gg W_{\text{band}}^c$.

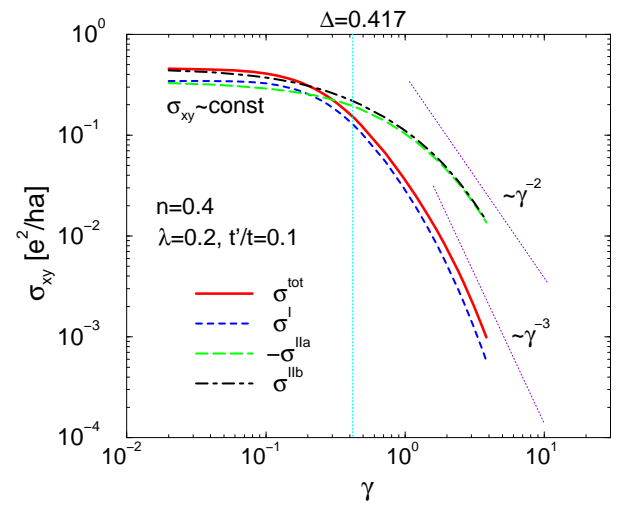


FIG. 7: (color online) γ -dependences of σ_{xy} ($= \sigma^{\text{tot}}$), σ_{xy}^I ($= \sigma^I$), σ_{xy}^{IIa} ($= \sigma^{IIa}$) and σ_{xy}^{IIb} ($= \sigma^{IIb}$), respectively. σ_{xy} shows a crossover behavior at $\gamma \sim \Delta$. It is shown that σ_{xy}^I reproduces a overall behavior of the total σ_{xy} for a wide range of γ .

We also study the γ -dependences of the longitudinal conductivity σ_{xx} . Figure 8 shows that the relations $\sigma_{xx} \propto \gamma^{-1}$ and $\sigma_{xx}^{Ia} \gg \sigma_{xx}^{Ib}$ hold well for a wide range of γ . The conductivity σ_{xx} does not show any clear crossover behavior at $\gamma \sim \Delta$. When $\gamma \sim W_{\text{band}}$, σ_{xx} seems proportional to $\gamma^{-1.5}$, and σ_{xx}^{Ib} is as large as σ_{xx}^{Ia} . Although eqs. (21) and (22) suggest that $\sigma_{xx} \propto \gamma^{-2}$ when $\gamma \gg W_{\text{band}}$, we could not find such a behavior for $\gamma \gtrsim W_{\text{band}}$.

Finally, we study the relation between the AHC and the resistivity $\rho = 1/\sigma_{xx}$. Figure 9 shows that σ_{xy} is independent of ρ when $\rho \lesssim 0.1$ [$\sim 100\mu\Omega\text{cm}$]. On the other hand, σ_{xy} starts to decrease for $\rho \gtrsim 0.1$ in proportion to ρ^{-2} . This crossover behavior of σ_{xy} at $\rho \sim 100\mu\Omega\text{cm}$ is observed universally by recent experiments on various transition metal ferromagnets by Asamitsu et al.[18].

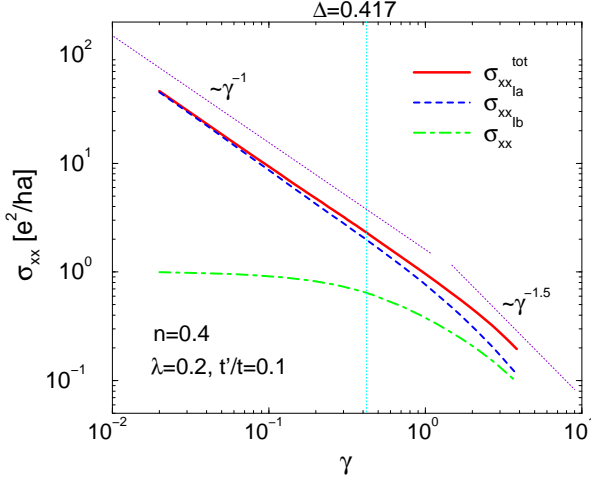


FIG. 8: (color online) γ -dependences of σ_{xx}^{Ia} , σ_{xx}^{Ib} and $\sigma_{xx} = \sigma_{xx}^{Ia} + \sigma_{xx}^{Ib}$.

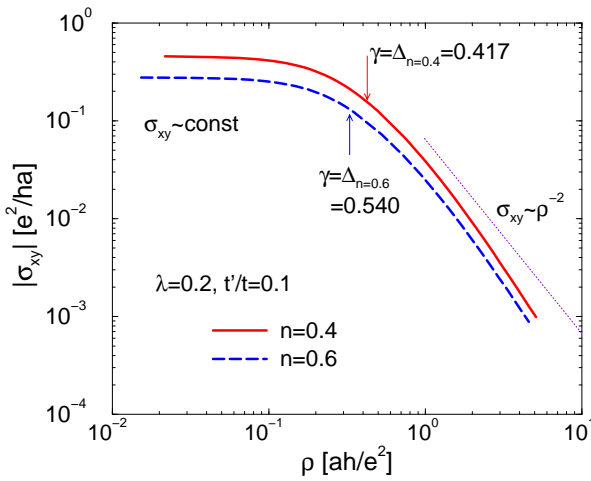


FIG. 9: (color online) Obtained relation between σ_{xy} and $\rho = 1/\sigma_{xx}$ for $n = 1.6$ and 0.4 . $\rho = 0.1$ corresponds to $100\mu\Omega\text{cm}$. It reproduces well the experimental universal “Asamitsu plot” for various transition metal ferromagnets, where $\sigma_{xy} = 10^2 \sim 10^3 \Omega^{-1} \text{cm}^{-1}$ for $\rho = 1 \sim 100\mu\Omega\text{cm}$, whereas $\sigma_{xy} \propto \rho^{-2}$ for $\rho \gg 100\mu\Omega\text{cm}$.

V. ANALYSIS OF ANOMALOUS HALL CONDUCTIVITY IN THE BAND-DIAGONAL REPRESENTATION

In this section, we analyze the intrinsic AHC in terms of the band-diagonal representation, which has been analyzed by many authors. We note that this representation is useful for the analysis of the AHC only when γ_α is orbital independent. In this representation, according to

eqs. (11) and (12),

$$\sigma_{xy}^I = \sum_{\mathbf{k}, l \neq m} \frac{1}{2\pi} v_x^{ml} v_y^{lm} \frac{1}{(\mu - E_{\mathbf{k}}^l + i\gamma)(\mu - E_{\mathbf{k}}^m - i\gamma)}, \quad (30)$$

$$\begin{aligned} \sigma_{xy}^{II} = & i \sum_{\mathbf{k}, l \neq m} \int_{-\infty}^{\mu} \frac{d\epsilon}{2\pi} v_x^{ml} v_y^{lm} \\ & \times \text{Im} \left\{ \frac{1}{(\epsilon - E_{\mathbf{k}}^l + i\gamma)^2} \frac{1}{(\epsilon - E_{\mathbf{k}}^m + i\gamma)} \right. \\ & \left. - \frac{1}{(\epsilon - E_{\mathbf{k}}^l + i\gamma)} \frac{1}{(\epsilon - E_{\mathbf{k}}^m + i\gamma)^2} \right\}, \end{aligned} \quad (31)$$

at zero temperature. Here, l and m are the band suffices, and we dropped the diagonal terms $l = m$ because they vanish identically. After performing the ϵ -integral in σ_{xy}^{II} , the Fermi sea term is expressed as $\sigma_{xy}^{IIa} + \sigma_{xy}^{IIb}$:

$$\begin{aligned} \sigma_{xy}^{IIa} = & \frac{i}{2\pi} \sum_{\mathbf{k}, l \neq m} v_x^{ml} v_y^{lm} \frac{1}{E_{\mathbf{k}}^l - E_{\mathbf{k}}^m} \\ & \times \text{Im} \left\{ \frac{E_{\mathbf{k}}^l + E_{\mathbf{k}}^m - 2\mu - 2i\gamma}{(E_{\mathbf{k}}^l - \mu + i\gamma)(E_{\mathbf{k}}^m - \mu - i\gamma)} \right\}, \end{aligned} \quad (32)$$

$$\begin{aligned} \sigma_{xy}^{IIb} = & \frac{-i}{\pi} \sum_{\mathbf{k}, l \neq m} v_x^{ml} v_y^{lm} \frac{1}{(E_{\mathbf{k}}^l - E_{\mathbf{k}}^m)^2} \\ & \times \text{Im} \left\{ \ln \left(\frac{E_{\mathbf{k}}^l - \mu - i\gamma}{E_{\mathbf{k}}^m - \mu - i\gamma} \right) \right\}. \end{aligned} \quad (33)$$

When γ is very small, they are given by

$$\sigma_{xy}^I = \frac{-i}{2} \sum_{\mathbf{k}, l \neq m} \delta(\mu - E_{\mathbf{k}}^l) \frac{v_x^{ml} v_y^{lm} - v_x^{lm} v_y^{ml}}{E_{\mathbf{k}}^l - E_{\mathbf{k}}^m}, \quad (34)$$

$$\sigma_{xy}^{IIa} = -\sigma_{xy}^I, \quad (35)$$

$$\sigma_{xy}^{IIb} = i \sum_{\mathbf{k}, l \neq m} f(E_{\mathbf{k}}^l) \frac{v_x^{ml} v_y^{lm} - v_x^{lm} v_y^{ml}}{(E_{\mathbf{k}}^l - E_{\mathbf{k}}^m)^2}. \quad (36)$$

Because $v_\mu^{lm} = J_\mu^{lm}/(E_{\mathbf{k}}^m - E_{\mathbf{k}}^l)$ and $J_\mu^{lm} = \langle \mathbf{k}, l | \partial/\partial k_\mu | \mathbf{k}, m \rangle$, σ_{xy}^{IIb} is equivalent to eq. (2.16) of ref. [12], or eq. (3) of ref. [24]. Based on eq. (36), When the Fermi energy lies in a gap, σ_{xy}^{IIb} is quantized when the Fermi energy lies in a gap [42]. In the metallic state, on the other hand, σ_{xy}^{IIb} is rewritten as the Fermi surface term due to the partial integral.

Off course, we can reproduce eqs. (26)-(28) by applying eqs. (34)-(36) to the present tight-binding model given in §II. In the band-diagonal representation ($E_{\mathbf{k}}^\alpha$; $\alpha = \pm$), we can show that the off-diagonal velocity is given by

$$\begin{aligned} v_x^{+-} = & -\{ |\alpha|^2 v_x^{xx} - \xi^{xy} (\xi^x - \xi^y) v_x^{xy} \\ & i\lambda v_x^{xy} |E_{\mathbf{k}}^+ - E_{\mathbf{k}}^-| \} / (|\alpha| |E_{\mathbf{k}}^+ - E_{\mathbf{k}}^-|), \end{aligned} \quad (37)$$

$$\begin{aligned} v_y^{+-} = & \{ |\alpha|^2 v_y^{yy} - \xi^{xy} (\xi^x - \xi^y) v_y^{xy} \\ & - i\lambda v_y^{xy} |E_{\mathbf{k}}^+ - E_{\mathbf{k}}^-| \} / (|\alpha| |E_{\mathbf{k}}^+ - E_{\mathbf{k}}^-|), \end{aligned} \quad (38)$$

and $v_\mu^{-+} = \{v_\mu^{+-}\}^*$. Therefore,

$$v_x^{\alpha\bar{\alpha}} v_y^{\bar{\alpha}\alpha} = -i\lambda \frac{v_x^{xx} v_y^{xy} + v_x^{xy} v_y^{yy}}{E_{\mathbf{k}}^\alpha - E_{\mathbf{k}}^{\bar{\alpha}}} + (\text{non A}_{1g} \text{ terms}), \quad (39)$$

where $\alpha = \pm$ and $\bar{\alpha} = -\alpha$. Substituting this result into eqs. (34)-(36), we obtain the same results given in §III.

VI. DISCUSSIONS

A. Summary of the Present Study

In the present paper, we studied the mechanism of the intrinsic AHE in transition metal ferromagnets based on the (d_{xz}, d_{yz}) -orbital tight-binding model. The origin of the anomalous velocity is the hopping integral between d_{xz} and d_{yz} orbitals, t' . By virtue of it, we could reproduce a typical experimental value of the AHC in ferromagnets; $10^2 \sim 10^3 \Omega^{-1} \text{cm}^{-1}$. Thus, the anomalous velocity due to atomic d -orbitals will be the main origin of the AHE in transition metal oxides. This fact has been overlooked in previous theoretical works based on electron gas models without atomic orbitals. We note that the present model breaks the parity symmetry $[(x, y) \rightarrow (-x, y)]$ due to $t' \neq 0$. This is a necessary condition for a spontaneous Hall effect [24, 44].

In accord with the present study, paramagnetic compound $\text{Ca}_{1.7}\text{Sr}_{0.3}\text{RuO}_4$ shows large AHE under the magnetic field [43]. Its magnitude is comparable with the large AHE in f -electron systems (such as UPt_3) which originates from the anomalous velocity due to atomic f -orbitals [26]. The Fermi surfaces of this compound are composed of t_{2g} -orbital (d_{xz} , d_{yz} , d_{xy} -orbitals); γ -band composed of d_{xy} -orbital is absent in the present (d_{xz}, d_{yz}) -tight-binding model. We will study the AHE of this compound in more detail based on the t_{2g} -orbital tight-binding model, which reproduces the bandstructure of $(\text{Ca}, \text{Sr})_2\text{RuO}_4$ accurately [23].

We derive a general expression for the AHC valid for any quasiparticle damping rate γ , by performing the analytic continuation carefully. [Equations (17), (18) and (19) for (d_{xz}, d_{yz}) -orbital model, and eqs. (30), (32) and (33) for a general model.] Using the general expression, we succeeded in explaining the experimental crossover behavior of the AHC in bad metals; σ_{xy} is constant for $\rho \lesssim 100 \mu\Omega\text{cm}$, whereas $\sigma_{xy} \propto \rho^{-2}$ for higher resistivity. This overall behavior is mainly given by the Fermi surface term, σ_{xy}^I , whose importance was intensively studied in ref. [26].

We stress that the intrinsic AHC in the present model is not a monotonic function with respect to $m_z = n_\downarrow$. In partial ferromagnets, the total AHC is given by

$$\sigma_{xy}(n_\uparrow, n_\downarrow) = \sigma_{xy}(\mu_\downarrow) - \sigma_{xy}(\mu_\uparrow) \quad (40)$$

where $\sigma_{xy}(\mu)$ is given by eq. (16), and $\mu_{\uparrow(\downarrow)}$ is the chemical potential for the electron density $n_{\uparrow(\downarrow)}$. We found that

the sign-change of σ_{xy} occurs in correspondence with sign of v_x^{xy} at \mathbf{k}^* . We expect that this result will explain the sign-change of the AHE in SrRuO_3 as a function of the magnetization. We comment that authors of ref. [24] found that a large value of AHC appears from σ_{xy}^{IIb} when Fermi level lies inside a narrow "anticrossing band gap", and they suggested that this mechanism accounts for a huge AHC in ferromagnets. However, this condition will be satisfied only for a narrow range of magnetization. The present model with (d_{xz}, d_{yz}) -orbitals can give an enough magnitude of the AHC, although band crossings are absent (except at $\mathbf{k} = (0, 0)$ and (π, π)). We stress that the AHC in the present model shows a sign change with respect to m_z , even if the topology of the Fermi surface is unchanged; see Fig. 5.

The relation $\sigma_{xy} = \sigma_{xy}^{IIb}$ (Berry curvature term) will not hold in usual metallic compounds: For example, in bad metals where γ is as large as the minimum band-splitting measured from the Fermi surface, Δ , the relations $\sigma_{xy} \approx \sigma_{xy}^I$ (Fermi surface term) and $|\sigma_{xy}^I| \gg |\sigma_{xy}^{II}|$ hold well for a wide range of γ as shown in fig. 7. Even in good metals, the relation $\sigma_{xy} = \sigma_{xy}^{IIb}$ is also invalid when (a) γ is \mathbf{k} -dependent, and/or (b) γ depends on band index, i.e., $\gamma_l/\gamma_m \neq 1$: In these cases, the Fermi surface term deviates from eq. (26) as shown in Appendix B and C.

In summary, the relation $\sigma_{xy} = \sigma_{xy}^{IIb}$ will hold only in good metals as well as when $\gamma_l(\mathbf{k}, \omega)$ is independent of l , \mathbf{k} and ω . On the other hand, the relation

$$\sigma_{xy} \approx \sigma_{xy}^I \quad (\text{Fermi surface term}) \quad (41)$$

will be universal in real metallic systems, since the Fermi sea terms almost cancel each other except for a special situation where μ lies inside a narrow anticrossing band gap. This result is consistent with recent theoretical work on metallic graphene [21]. For a quantitative study of the intrinsic AHC, however, we have to calculate σ_{xy}^I , σ_{xy}^{IIa} and σ_{xy}^{IIb} on the same footing. This is also important conclusion in this paper.

Finally, we comment that the present (d_{xz}, d_{yz}) -tight binding model in a paramagnetic state shows a finite spin Hall conductivity (SHC) σ_{xy}^z , that is, σ_z -spin current along y -axis occurs under the electric field along x -axis. σ_{xy}^z is given by $(-\hbar/e)$ times eqs. (16). As shown in Fig. 5, σ_{xy}^z reaches 0.6 $[(\hbar/e)(e^2/ha)] \sim 600$ $[\text{he}^{-1} \cdot \Omega^{-1} \text{cm}^{-1}]$ for $a = 4\text{\AA}$, which is almost one order of magnitude larger than typical SHC in semimetals [22]. In later publications, we will study the spin Hall effect in more detail [23].

B. Comparison with Experiments: Transition Metals

Asamitsu et al. examined the experimental relation between the AHC and the resistivity ρ in various ferromagnets. They observed the dissipation-less intrinsic AHC in the intermediate conducting region with

$\rho = 1 \sim 100 \mu\Omega\text{cm}$. In the bad metal region, σ_{xy} is proportional to ρ^{-2} , which is well explained in the present study. We found this crossover at $\sim 100 \mu\Omega\text{cm}$ occurs when $\gamma \sim \Delta$. According to Fig. 8, $100 \mu\Omega\text{cm}$ corresponds to $\Delta \sim 0.2 \approx 800\text{K}$. Another crossover to the good metal region ($\sim 1 \mu\Omega\text{cm}$) seems to be rather complex: It might be due to the extrinsic AHE or a phenomenon related to the normal Hall effect.

Recently, S. Onoda et al. [45] calculated both the intrinsic AHC [12, 26] and the extrinsic AHC [13, 19] in a Rashba-type 2D electron gas (2DEG) model. They claimed that the extrinsic-intrinsic crossover occurs when $\gamma \sim \Delta$, and tried to explain the crossover at $\rho \sim 1 \mu\Omega\text{cm}$ observed by Asamitsu. However, it will not be true because $1 \mu\Omega\text{cm}$ corresponds to $\gamma \sim 10^{-3} \approx 8\text{K}$, which is too small for a realistic value of Δ . (see Fig. 8.) We stress that Inoue et al. [46] proved that the intrinsic AHE in a Rashba model almost vanishes due to the cancellation by the current vertex correction (CVC) by impurities. On the other hand, we have checked that the CVC for anomalous velocity is absent in the present (d_{xz}, d_{yz})-orbital model within the Born approximation, when the impurity potential is delta-functional. By this reason, the intrinsic AHC obtained in the present work is not modified by the CVC. We conclude that the present model with atomic d -orbital degrees of freedom is essential for a realistic study of AHE in ferromagnets.

C. Comparison with Experiments: Heavy Fermions

In paramagnetic heavy fermion (HF) systems, the Hall coefficients takes huge values due to the AHE, since the uniform susceptibility $M/B = \chi$ in HF is prominently enhanced by the strong Coulomb interaction. In HF systems, the large quasiparticle damping rate \hbar/τ comes from the strong electron correlation (or Kondo resonance). In the early stage, Coleman et al [38] and Fert and Levy [39] developed theories of the extrinsic AHE: developed theories of extrinsic AHE: They studied the extrinsic mechanism based on the f -electron impurity Anderson models with d -orbital channel, and predicted the relation $R_H \propto \chi\rho$ above T_0 . They assumed that the impurity Anderson models is applicable for the study of AHE in periodic systems if $T > T_0$.

On the other hand, Kontani and Yamada found that the $J = 5/2$ periodic Anderson model (PAM) gives a

large intrinsic AHC [26, 27]. They predict that $\sigma_{xy}^a \propto \chi$ below T_0 , whereas $\sigma_{xy}^a \propto \chi\rho^{-2}$ above T_0 . We expect this intrinsic AHE is widely observed since the $J = 5/2$ PAM is a well-established effective model for Ce-based HF systems: For example, it could explain a large Van-Vleck susceptibility in Kondo insulator [47, 48].

There remain a lot of future works to be done about the AHE in HF systems. For example, Nakajima et al. found that the AHC in two-dimensional HF system, CeMIn₅ (M=Co,Rh,Ir) is negligibly small [49, 50]. In this compound, strong temperature dependence of R_H is given by the normal Hall effect, due to the effect of the current vertex corrections (or backflow) in nearly antiferromagnetic Fermi liquids [51, 52]. In addition, an interesting field-direction dependence of AHC is found in CeCu₆ or CeCu_{5.9}Au_{0.1} [53]. Theoretical studies on these experimental results will give us important hints to understand the electronic states.

Acknowledgments

We are grateful to J. Inoue, Y. Tanaka, D.S. Hirashima, M. Sato and H. Sato for enlightening discussions. We also thank H. Fukuyama for sending us his thesis [15].

APPENDIX A: AHC WITHIN THE BORN APPROXIMATION; EFFECT OF OFFDIAGONAL ELEMENT OF γ

In previous sections, we studied the AHC by assuming that $\text{Im}\hat{\Sigma}$ is diagonal with respect to atomic orbital. This assumption seems to be justified since $|\text{Im}\Sigma_{1,1}| \gg |\text{Im}\Sigma_{1,2}|$ when ls -coupling constant λ is much smaller than bandwidth W_{band} . [When $\lambda = 0$, $\text{Im}\Sigma_{1,2} = 0$ since the local Green function $\hat{g}(\omega) = \sum_{\mathbf{k}} \hat{G}_{\mathbf{k}}(\omega)$ is diagonal due to the orthonormality of d -orbitals.] Here, we derive the AHC within the Born approximation, by taking both the diagonal and off-diagonal elements of $\text{Im}\hat{\Sigma}$. As a result, it is confirm that the off-diagonal element is negligible in calculating the AHC in the present model.

In the Born approximation, the Green function is given by

$$\hat{G}^R(\omega) = \frac{1}{d(\omega)} \begin{pmatrix} \omega + \mu - \xi_{\mathbf{k}}^y + i\gamma & \alpha_{\mathbf{k}}^0 + i\lambda(1 + g - ih) \\ \alpha_{\mathbf{k}}^0 - i\lambda(1 + g - ih) & \omega + \mu - \xi_{\mathbf{k}}^x + i\gamma \end{pmatrix}, \quad (\text{A1})$$

$$\hat{G}^A(\omega) = \frac{1}{d(\omega)} \begin{pmatrix} \omega + \mu - \xi_{\mathbf{k}}^y - i\gamma & \alpha_{\mathbf{k}}^0 + i\lambda(1 + g + ih) \\ \alpha_{\mathbf{k}}^0 - i\lambda(1 + g + ih) & \omega + \mu - \xi_{\mathbf{k}}^x - i\gamma \end{pmatrix}, \quad (\text{A2})$$

where γ , g and h come from the self-energy correction in

the self-inconsistent Born approximation:

$$\begin{aligned} i\gamma &\equiv -i\text{Im}\Sigma_{1,1}^R(0) \\ &= -in_{\text{imp}}I^2\text{Im} \sum_{\mathbf{k}} \frac{\mu - \xi_{\mathbf{k}}^y}{d^R(0)}, \end{aligned} \quad (\text{A3})$$

$$i\lambda(g - ih) \equiv \Sigma_{1,2}^R(0)$$

where n_{imp} is the impurity concentration and I is the impurity potential. Therefore, $\gamma = \pi n_{\text{imp}} I^2 N(0)/2 \sim n_{\text{imp}} I^2 / W_{\text{band}}$, where $N(0)$ is the DOS at the Fermi level. In the same way, we can estimate that $g, h \sim n_{\text{imp}} (I/W_{\text{band}})^2 \sim \gamma/W_{\text{band}} \ll 1$.

We can derive the expression for the AHC by inserting eqs. (A1) and (A2) into the Streda formula in §III, in the same way of deriving eqs. (13) and (14). Using the square lattice symmetry of the present model, the Fermi surface term at zero temperature is given by

$$\sigma_{xy}^I = \frac{2\lambda}{\pi} \sum_{\mathbf{k}} \frac{v_x^{xx} v_y^{xy}}{d^R(0) d^A(0)} [\gamma(1+g) + h(\mu - \xi^y)], \quad (\text{A5})$$

Since the main contribution in the \mathbf{k} -summation comes from $\mathbf{k} \sim \mathbf{k}^*$, where \mathbf{k}^* represents the position of the minimum band-splitting Δ , as shown in fig. 3. Since $h|\mu - \xi^y| \sim h\Delta \ll \gamma$ at $\mathbf{k} = \mathbf{k}^*$, the second term of eq. (A5) is negligible. Therefore, the correction due to off-diagonal element of the self-energy correction, $i\lambda(g - ih)$, is very small. As a result, eq. (13) is justified in the Born approximation.

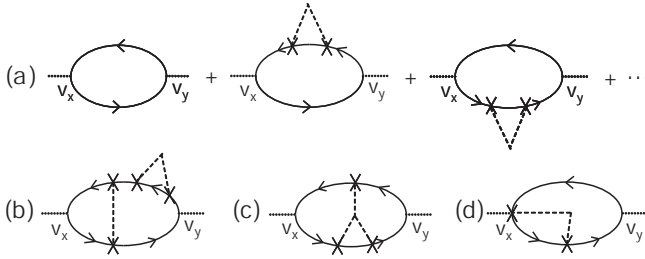


FIG. 10: (a) Diagrammatic expression for the intrinsic AHC given in eq. (A5). Self-energy correction due to impurity scattering is not diagonal when $\lambda \neq 0$. (b) and (c) represent the Born and the second Born approximation, respectively. The latter gives the skew scattering extrinsic AHE when the impurity potential is non-local. (d) represents the side jump extrinsic AHC.

Figure 10 (a) represents the intrinsic AHC given in eq. (A5). In good metals, the diagonal self-energy correction does not affect the AHC, and the AHC due to off-diagonal self-energy correction is negligible as we discussed above. In addition, current vertex correction (CVC) term (b) also exists in the Born approximation. Figure (c) and (d) represent other CVC terms which gives the extrinsic AHC: (c) gives the skew scattering extrinsic AHC that is proportional to σ_{xx} , and (d) represents the side-jump extrinsic AHC term that is proportional to $\{\sigma_{xx}\}^0$, respectively. The latter is caused by the lateral displacement of the wave-packet during the scattering, which is theoretically expressed by the modification of velocity operator due to impurity potential [17, 19]. In the present model, (b)-(d) vanish identically in the case of local impurity potential. In contrast, extrinsic AHC occurs by local impurity potential in 2D electron gas models when the ls -coupling term is \mathbf{k} -dependent [16].

APPENDIX B: AHC WHEN γ IS MOMENTUM DEPENDENT

In §III, §IV and §V, we have neglected the momentum dependences of the damping rate γ to simplify the discussion. However, this assumption is not realistic because $\text{Im}\Sigma_{\mathbf{k}}(0)$ is usually \mathbf{k} -dependent. In this appendix, we study the AHE by taking the \mathbf{k} -dependence of γ into account. Then, we have to distinguish $\gamma_x = \text{Im}\Sigma^{xx}(-i0)$ and $\gamma_y = \text{Im}\Sigma^{yy}(-i0)$. We show that the expression for σ_{xy}^I in eq. (26) could be changed prominently when the \mathbf{k} -dependence of γ is taken into account.

Along with the derivation of eq. (13), we obtain the expression for σ_{xy}^I in the present case:

$$\sigma_{xy}^I = \frac{\lambda}{\pi} \sum_{\mathbf{k}} \frac{v_x^{xx} v_y^{xy} \gamma_y + v_x^{xy} v_y^{yy} \gamma_x}{d^R(0) d^A(0)}, \quad (\text{B1})$$

where

$$d^R(0) d^A(0) = ((\mu - E_{\mathbf{k}}^+)^2 + \gamma_+^2)((\mu - E_{\mathbf{k}}^-)^2 + \gamma_-^2). \quad (\text{B2})$$

When both γ_x and γ_y are very small,

$$\gamma^{\pm} = \frac{\gamma_x + \gamma_y}{2} \left(1 \pm \frac{\xi^x - \xi^y}{E_{\mathbf{k}}^+ - E_{\mathbf{k}}^-} \frac{\gamma_x - \gamma_y}{\gamma_x + \gamma_y} \right). \quad (\text{B3})$$

In this case, eq. (B1) is given by

$$\sigma_{xy}^I = \lambda \sum_{\mathbf{k}} \frac{v_x^{xx} v_y^{xy} \gamma_y + v_x^{xy} v_y^{yy} \gamma_x}{(E_{\mathbf{k}}^+ - E_{\mathbf{k}}^-)^2} \times \left[\delta(\mu - E_{\mathbf{k}}^+) \frac{1}{\gamma_+^2} + \delta(\mu - E_{\mathbf{k}}^-) \frac{1}{\gamma_-^2} \right] \quad (\text{B4})$$

When γ_{μ} is momentum dependent, $\gamma_{x(y)}/\gamma^+ \neq 1$ except for $|k_x| = |k_y|$. Therefore, eq. (B4) is not equal to eq. (26) even in good metals ($\gamma_x, \gamma_y \rightarrow 0$).

In general, the momentum dependence (and the band-dependence) of γ could give rise to a nontrivial modulation of the AHC due to the Fermi surface term, σ_{xy}^I . This effect will be prominent in strongly correlated electron systems like high- T_c cuprates and heavy Fermion systems. On the other hand, the Fermi sea term σ_{xy}^{II} , which is given by eqs. (27) and (28), is satisfied when $\gamma_x, \gamma_y \rightarrow 0$, even if $\gamma_x/\gamma_y \neq 1$.

APPENDIX C: CALCULATION OF AHC WHEN γ IS BAND DEPENDENT

As shown in Appendix B, we have shown that the expression for Fermi surface term σ_{xy}^I given in eq. (26) is modified by the \mathbf{k} -dependence of γ . In this section, we explain that eq. (26) is also changed when γ depends on bands. This fact was already pointed out in Appendix D of ref. [26]. Here, we derive the first order term of

σ_{xy}^I with respect to the ls -coupling, and correct a mistake in Appendix D of ref. [26]. By extracting a single ls -coupling term from eq. (30), we obtain

$$\begin{aligned}\sigma_{xy}^I &= \frac{\lambda}{2\pi} \sum_{\mathbf{k}, l \neq m} G_l^R G_l^A \\ &\times [v_x^{ll} (G_m^R v_y^{ml} \langle l | l_z | m \rangle + G_m^A v_y^{lm} \langle m | l_z | l \rangle) \\ &+ (v_x^{lm} G_m^R \langle m | l_z | l \rangle + v_x^{ml} G_m^A \langle l | l_z | m \rangle) v_y^{ll}]\end{aligned}\quad (C1)$$

where $G_l^R = (\mu - E_{\mathbf{k}}^l + i\gamma_l)^{-1}$ and v_{μ}^{lm} are the Green function and the velocity without ls -coupling term. The diagrammatic expression is given in fig. 4 (b). Using the relation $\langle l | l_z | m \rangle = -\langle m | l_z | l \rangle$ and $v_{\mu}^{lm} = v_{\mu}^{ml}$, we obtain that

$$\begin{aligned}\sigma_{xy}^I &= \frac{\lambda}{2\pi} \sum_{\mathbf{k}, l \neq m} G_l^R G_l^A (G_m^R - G_m^A) \langle l | l_z | m \rangle \\ &\times [v_x^{ll} v_y^{lm} - v_x^{lm} v_y^{ll}].\end{aligned}\quad (C2)$$

When γ_l is very small,

$$\begin{aligned}G_l^R G_l^A (G_m^R - G_m^A) &= \frac{2\pi i}{(E_{\mathbf{k}}^l - E_{\mathbf{k}}^m)^2} \\ &\times \left[\delta(\mu - E_{\mathbf{k}}^l) \frac{\gamma_m}{\gamma_l} + \delta(\mu - E_{\mathbf{k}}^m) \right].\end{aligned}\quad (C3)$$

In this case, eq. (C2) is given by

$$\begin{aligned}\sigma_{xy}^I &= \lambda \sum_{\mathbf{k}, l \neq m} \left[\delta(\mu - E_{\mathbf{k}}^l) \frac{\gamma_m}{\gamma_l} + \delta(\mu - E_{\mathbf{k}}^m) \right] \\ &\times \frac{i \langle l | l_z | m \rangle}{(E_{\mathbf{k}}^l - E_{\mathbf{k}}^m)^2} [v_x^{ll} v_y^{lm} - v_x^{lm} v_y^{ll}].\end{aligned}\quad (C4)$$

In summary, σ_{xy}^I depends on the ratio of γ_m/γ_l . σ_{xy}^I could take a huge value if γ_l differs much from band to band. This fact was already pointed out by ref. [26]. On the other hand, eqs. (27) and (28) for the Fermi sea term σ_{xy}^{II} is satisfied when $\gamma_l \rightarrow 0$, even if $\gamma_m/\gamma_l \neq 1$. The present result will be valid even if the ls -coupling is treated unperturbatively, as done in §II - §IV. In fact, Fig. 6 shows that σ_{xy} is approximately linear-in- λ for $\lambda < 0.2$.

In Appendix D of ref. [26], $E_{\mathbf{k}}^m$ in $\delta(\mu - E_{\mathbf{k}}^m)$ was replaced with $E_{\mathbf{k}}^l$ by mistake. Thus, eq. (C4) is not equal to the KL's term which is given by [eq. (3.5)] $\times(2/mE_b)$ in ref. [12] with $(a, b) = (x, y)$. This difference is natural since the former and the latter are the Fermi surface term and the Fermi sea term, respectively.

[1] S. Yoshi, S. Iikubo, T. Kageyama, K. Oda, Y. Kondo, K. Murata and M. Sato: J. Phys. Soc. Jpn. **69** (2000) 3777.
[2] Y. Yasui, T. Kageyama, T. Moyoshi, M. Soda, M. Sato and K. Kakurai: J. Phys. Soc. Jpn. **75** (2006) 084711.
[3] Y. Taguchi and Y. Tokura: Phys. Rev. B **60** (1999) 10280.
[4] Y. Taguchi, Y. Oohara, H. Yoshizawa, N. Nagaosa and Y. Tokura: Science **291** (2001) 2573.
[5] W.L. Lee, S. Watauchi, V.L. Miller, R.J. Cava and N.P. Ong: Science **303** 1647.
[6] L. Klein, J.R. Reiner, T.H. Geballe, M.R. Beasley, and A. Kapitulnik: Phys. Rev. B **61** (2000) R7842.
[7] M. Izumi, K. Nakazawa, Y. Bando, Y. Yoneda and H. Terauchi: J. Phys. Soc. Jpn. **66** (1997) 3893.
[8] H. Sato, T. Kumano, Y. Aoki, T. Kaneko and R. Yamamoto: J. Phys. Soc. Jpn. **62** (1993) 416.
[9] C.L. Canedy, X.W. Li and G. Xiao: Phys. Rev. B **62** (2000) 508.
[10] G. Tatara and H. Kawamura: J. Phys. Soc. Jpn. **71** (2002) 2613.
[11] H. Kawamura: Phys. Rev. Lett. **90** (2003) 047202.
[12] R. Karplus and J. M. Luttinger: Phys. Rev. **95** (1954) 1154.
[13] J. Smit: Physica **24** (1958) 39.
[14] J. M. Luttinger: Phys. Rev. **112** (1958) 739.
[15] H. Fukuyama, Ph. D thesis, 1970 (unpublished).
[16] N.A. Sinitsyn, A.H. MacDonald, T. Jungwirth, V.K. Dugaev and J. Sinova: cond-mat/0608682.
[17] L. Berger, Phys. Rev. B **2** (1970) 4559.
[18] T. Miyasato, N. Abe, T. Fujii, A. Asamitsu, S. Onoda, Y. Onose, N. Nagaosa, Y. Tokura: cond-mat/0610324.
[19] A. Crepieux and P. Bruno: Phys. Rev. B **64** (2001) 014416.
[20] P. Streda: J. Phys. C: Solid State Phys. **15** (1982) L717.
[21] N.A. Sinitsyn, J.E. Hill, H. Min, J. Sinova and A.H. MacDonald: Phys. Rev. Lett. **97** (2006) 106804.
[22] S. Murakami, N. Nagaosa and S.C. Zhang: Science **301** (2003) 1348.
[23] H. Kontani, T. Tanaka, D.S. Hirashima, K. Yamada and J. Inoue, cond-mat/cond-mat/0702447.
[24] M. Onoda and N. Nagaosa: J. Phys. Soc. Jpn. **71** (2002) 19.
[25] G. Sundaram and Q. Niu: Phys. Rev. B **59** (1999) 14915.
[26] H. Kontani and K. Yamada: J. Phys. Soc. Jpn. **63** (1994) 2627.
[27] H. Kontani and K. Yamada: J. Phys. Soc. Jpn. **66** (1997) 2252.
[28] Y. Ōnuki, T. Yamayoshi, I. Ukon, T. Komatsubara, A. Umezawa, W. K. Kwok, G. W. Crabtree and D. G. Hinks: J. Phys. Soc. Jpn. **58** (1989) 2119.
[29] Y. Ōnuki, T. Yamayoshi, T. Omi, I. Ukon, A. Kobori and T. Komatsubara: J. Phys. Soc. Jpn. **58** (1989) 2126.
[30] M. Miyazawa, H. Kontani and K. Yamada: J. Phys. Soc. Jpn. **68** (1999) 1625.
[31] Y. Yao, L. Kleinman, A.H. MacDonald, J. Sinova, T. Jungwirth, D.S. Wang, E. Wang and Q. Niu: Phys. Rev. Lett. **92** (2004) 037204.
[32] Z. Fang et al.: Science **302** (2003) 92.
[33] K.K. Ng and M. Sigrist, Europhys. Lett. **49**, 473 (2000).
[34] T. Nomura and K. Yamada: J. Phys. Soc. Jpn. **71** (2002) 404; T. Nomura and K. Yamada: J. Phys. Soc. Jpn. **71** (2002) 1993;

- [35] Y. Yanase and M. Ogata, *J. Phys. Soc. Jpn.* **72**, 673 (2003).
- [36] N.A. Sinitsyn, Q. Niu, J. Sinova and K. Nomura: cond-mat/0502426.
- [37] J. Kondo: *Prog. Theor. Phys.* **27** (1962) 772.
- [38] P. Coleman, P. W. Anderson and T. V. Ramakrishnan: *Phy. Rev. Lett.* **55** (1985) 414.
- [39] A. Fert and P. M. Levy: *Phy. Rev. B* **36** (1987) 1907.
- [40] J. Slater and G. Koster, *Phys. Rev.* **94**, 1498 (1954).
- [41] H. Nakano: *Int. J. Mod. Phys. B* **7** (1993) 2397.
- [42] D.J. Thouless, M. Kohmoto, M.P. Nightingale and M. den Nijs: *Phys. Rev. Lett.* **49** (1982) 405.
- [43] J. Jin et al., cond-mat/0112405.
- [44] F.D.M. Haldane: *Phys. Rev. Lett.* **61** (1998) 2015.
- [45] S. Onoda, N. Sugimoto and N. Nagaosa: *Phys. Rev. Lett.* **97** (2006) 126602.
- [46] J. Inoue, T. Kato, Y. Ishikawa, H. Itoh, G.E.W. Bauer and L.W. Molenkamp: *Phys. Rev. Lett.* **97** (2006) 046604.
- [47] H. Kontani and K. Yamada: *J. Phys. Soc. Jpn.* **65** (1996) 172.
- [48] H. Kontani and K. Yamada: *J. Phys. Soc. Jpn.* **66** (1997) 2232.
- [49] Y. Nakajima, K. Izawa, Y. Matsuda, S. Uji, T. Terashima, H. Shishido, R. Settai, Y. Onuki and H. Kontani, *J. Phy. Soc. Jpn.* **73** (2004) 5.
- [50] Y. Nakajima, K. Izawa, Y. Matsuda, K. Behnia, H. Kontani, M. Hedo, Y. Uwatoko, T. Matsumoto, H. Shishido, R. Settai and Y. Onuki: *J. Phy. Soc. Jpn.* **75** (2006) 023705.
- [51] H. Kontani, K. Kanki and K. Ueda: *Phys. Rev. B* **59** (1999) 14723.
- [52] H. Kontani and K. Yamada: *J. Phy. Soc. Jpn.* **74** (2005) 155.
- [53] T. Namiki, H. Sato, H. Sugawara, Y. Aoki, R. Settai and Y. Onuki: preprint.